A comparative study on the Refractive Index of Silk Protein Thin Films and Silk Protein Resist Thin Films.

Alessio Bucciarelli[a], Viviana Mulloni[b], Devid Maniglio[a], Ramendra K.Pal[c], Vamsi Yadavalli[c], Antonella Motta[a], Alberto Quaranta[a]

[a] Department of Industrial Engineering, University of Trento, Via Sommarive 9, 38123 Trento (TN), Italy

[b] Micro System Technology group, Fondazione Bruno Kessler, Via Sommarive 18, 38123, Trento (TN), Italy

[c] BioNano Laboratory, Department of Chemical and Life Science Engineering, Virgina Commonwealth University, 601 W. Main Street Richmond, Virginia 23284-3018.

Keywords: Silk Fibroin, Silk Sericine, Fibroin Photocrosslinkable Photoresist, Sericine Photocrosslinkable Photoresist, Refractive Index, Silk Optic, Thin Film.

Highlights

- Spin Coating has been optimized to give Silk Protein thin films with an extreme low roughness.
- Refractive indexes were determined by ellipsometry in a 400 - 1600 nm range using Sellmaier and Cauchy dispersion laws.
- Refractive Index of Silk Fibroin Photoresist and Silk Sericine Photoresist thin films prepared by Formic Acid solution have been characterized.
- Refractive Index of Silk Fibroin has been characterized for films prepared form Water solution and Formic Acid solution, the difference in the RI has been attributed to the secondary structure modification.
- Refractive Index of Silk Sericine thin films prepared from Formic Acid solution have been characterized.

Abstract

In the last two decades Silk Fibroin due to the combination of unique properties has been exploited as optical materials in biological application. Recently a protocol has been developed to produce a Silk Fibroin resist crosslinkable via UV photolithography. The same protocol has been applied to Sericine to develop a Silk Sericine resist. Despite the use of these materials to develop micro patterns on silicon and glass surfaces, and self-standing micro optical components, their refractive index has never been characterized. In this work, optimizing a method to obtain extremely smooth and thin films we were able to characterize by ellipsometry the refractive index of both Sericine and Fibroin Resist. In addition, we report as reference the refractive index of: silk sericine obtained from formic acid solution and silk fibroin obtained both from formic acid and water solutions. The parameters of the Sellmaier and Cauchy dispersion laws have been determined. The differences of refractive index of Silk Fibroin films produced by different solvents has been explained examining the change in the protein secondary structure, moreover a complete morphological study of the films has been conducted.

Graphical abstract

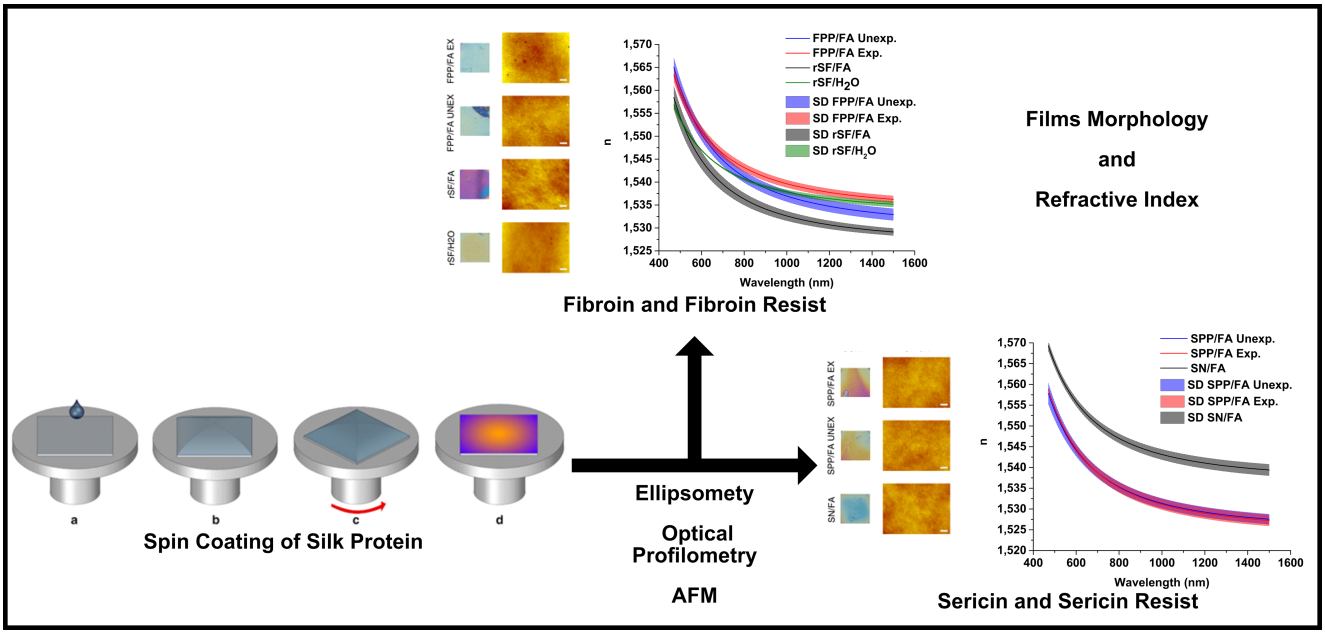

1. Introduction

For thousand years silk has been used for producing luxury textile with an exceptional texture, robustness, and shine. In the last two decades, silk fibroin has been investigated by the scientific community for different technological applications, namely tissue engineering [1][2], drug delivery [3][4][5] and, more in general, in the biomedical field [6][7]. Recently the unique combination of silk fibroin properties [8][9] such high transparency, mechanical robustness [10] and the possibility to be patterned, has led to the development of several bio-optical devices, spanning from optical waveguides [11][12][13] to optical sensors [14][15][16][13]. Another bioproduct of cocoons, sericin, has been used in many biomedical [17][18][19][20] applications, but to date, due to the yellowish color of thick (more than 10 μm) free-standing films, it was never used for applications in the fabrication of optical systems.

In recent years the development of silk proteins based UV-crosslinkable photoresists, has further expanded their use. To obtain UV sensitive layers, methacrylate groups have been grafted to the protein amino-acidic chain through a conjunction reaction. This procedure allowed the production of both fibroin photocrosslinkable photoresist (FPP) [21] and sericin photocrosslinkable photoresist (SPP) [22] for the realization of protein micropatterns on silicon and glass surfaces and suitable for the production of free-standing flexible micro-optical components [23]. Recently, using the same modification procedure on light chain fibroin (LC fibroin) an improved resist has been developed [24], allowing the formation of a pattern with a resolution of 1.51 μm and a roughness of 2.3 nm. These results pave the way to realize new, silk proteins based optical devices.

The most important parameter for the design of optical devices is the refractive index (RI). To date, in nearly all the literature the RI of silk fibroin materials have been characterized at a single wavelength, namely 630 nm [11][12] and 500nm [25] giving a value respectively around 1.54 and 1.52 (80% Relative Humidity). Since this RI is higher than soda-lime glass (RI = 1.5), optical waveguides [11] have been fabricated with fibroin coatings on glass substrates. Recently, a core-

cladding waveguide [12] have been fabricated exploiting the RI difference between two different forms of silk fibroin materials: hydrogel for the cladding (RI = 1.34) and solid form for the core (RI = 1.54). An attempt to use silk fibroin fiber as optical fiber right after the degumming process has been conducted, but without reporting any RI numerical evaluation [26]. The RI change due to electron [27] and γ [28] irradiation of silk fibroin self-standing films has been investigated using UV-Vis spectroscopy, a methodology commonly used for thick samples. In this case, the entire RI trend over the visible spectrum has been calculated, but the RI data at 630 nm resulted to be incoherent with previous works. This incoherency probably arises from the method used, that provides good results only in case of samples with perfectly flat surfaces, not achievable on self-standing fibroin films. Only recently, ellipsometric analyses on a broad spectral range (250-1750 nm) have been performed on thin films of titania – silk fibroin nanocomposites [29], which have been used in combination with pure fibroin thin films to develop an alternating stack usable as a colorimetric humidity sensor [25]. Similar RI measurement has also been conducted by Perotto et al. on films produced with fibroin produced by several worm species [30]. In this work, the authors report a detailed analysis on the refractive index of several types of coatings, some microns thick, produced with water-based fibroin, evidencing how the RI value does not depend on the degumming procedure and how it increases in β-crystalline structures.

Despite these characterizations, several investigations are still needed. Since now, for example, only materials produced starting from water-based silk fibroin solutions have been used, excluding any alternative solvent that could be beneficial for the fabrication process but, together, could deeply affect the fibroin secondary structure [31] and, consequently, the refractive index. It is the case of the use of formic acid (FA) whose use could lead to the formation of a different amount of crystalline compact secondary structure in the films obtained by casting. Furthermore, sericin, SPP, and FPP refractive indexes have never been characterized so far.

Recently our group proposed a method to obtain optical thin films of high quality based on the spin coating on silicon substrates of silk protein resist dispersed in FA [32]. This method allowed obtaining exceptionally flat and uniform films with higher transparency with respect to films obtained from fibroin solutions in hexafluoroisopropanol (HFP). For the produced films, RI measured at 633 nm (1.558) was slightly higher than the RI reported in the literature for silk fibroin films (1.54).

In this work, by optimizing the spin coating procedure we obtained films that show an extremely low roughness both in nanometric and micrometric areas. The refractive index of fibroin, sericin, FPP and SPP thin films cast from both water and FA solutions were measured using spectroscopic ellipsometry. An increment of FPP refractive index with respect to that of water-based fibroin was revealed, while the modification of silk sericin strongly decreases its RI. After UV treatment FPP films showed a further little increment of RI; instead, SPP films exhibited no variation of RI.

2. Materials and Methods

2.1 FPP and SPP synthesis

Extraction and purification of silk fibroin from silkworm cocoon was conducted following a well-established protocol [33]. A method previously described has been used to synthesize FPP and SPP [21][22]. Briefly, lyophilized fibroin was dissolved in a 1 M solution of Lithium Chloride (LiCl, Sigma Aldrich) in Dimethyl Sulfoxide (DMSO, Sigma Aldrich) under N_2 flux at the controlled temperature of 60°C until the complete dissolution. A stoichiometric quantity of 2-isocyanoetil methacrylate (IEM, Sigma Aldrich) was added to the solution to allow the conjugation reaction. After 4 h of reaction under stirring at 60 °C, cold ethanol was added to precipitate the functionalized protein. A washing and centrifuging procedure was repeated 5 times using a cold mixture of 50% acetone (Fisher Scientific) and 50% absolute ethanol (EtOH, Carlo Erba Reagents). The collected product was lyophilized for 48 h to obtain a yellowish powder. The same process, using a stoichiometric

quantity of IEM in the reaction, was used to obtain the SPP powder from pure sericin (Wako Chemicals).

2.2. Solutions preparation

To obtain thin films by spin coating suitable for the ellipsometric analysis, a low concentration of protein in solution is a preliminary requirement. Our method was optimized using protein resist solutions with a concentration of 1.5 wt.% in FA (FPP/FA and SPP/FA). The aqueous solution of silk fibroin (rSF/H_2O) was obtained by dilution of a 5 wt.% water solution of silk fibroin, obtained following the protocol described elsewhere [33], to 2% adding water. FA solution of silk fibroin (rSF/FA) was obtained dissolving a calculated amount of lyophilized silk fibroin in FA to obtain a 2 wt.% concentrated solution. Sericin solutions with 2 wt.% concentration in FA (SN/FA) were prepared by solubilization of a calculated amount of pure sericin. The concentrations of rSF/H_2O, rSF/FA, and SN/FA solutions were higher with respect to FPP/SA and SPP/FA in order to obtain reference films with a thickness comparable with silk protein resist films.

2.3. Substrate preparation

Protein thin films were deposited on silicon substrates to perform ellipsometric measurement using the method previously developed [32]. To allow a good protein adhesion and a better thickness uniformity, surfaces were functionalized using an acrylate compound. The initial surface cleaning has been conducted for 1 h in ambient condition using a piranha solution (3 part of H_2SO_4 98% Sigma Aldrich, 1 part of H_2O_2 30% Sigma Aldrich). Subsequently, cleaned surfaces were functionalized using a chemical vapor deposition (CVD) technique, exposing them 3-(trichlorosilyl) propyl methacrylate (TPM, Sigma Aldrich) in a desiccator for 14 h under vacuum. To eliminate the excess of deposited TPM treated surfaces were washed using hexane and water.

2.4. Film preparation

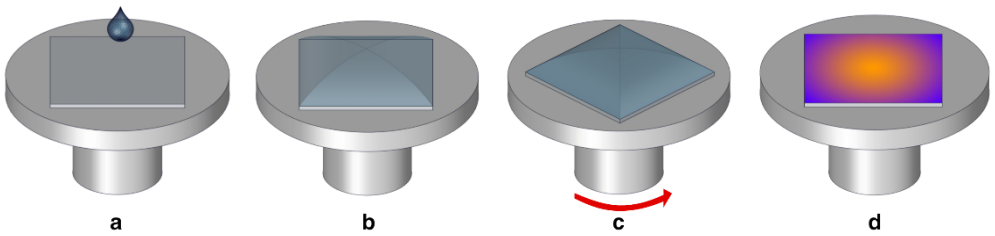

Fig. 1: modified spin coating process: **a** deposition of 70 µL of silk protein solution with low concentration, **b** *delay time of 5 minutes in a closed chamber under nitrogen flux,* **c** *spinning and,* **d** *evaporation. This process allows the production of very smooth surfaces suitable for ellipsometry measurements.*

The films preparation process has been conducted inside a clean room with controlled temperature and humidity (T = 21 °C, H = 50%), to reduce as much as possible the environmental variability. Protein films have been made using a Laurell WS-650 spin coater and a specifically developed protocol (**Fig. 1**). Briefly, 70 µL of a solution with a protein concentration of 1.5% or 2% was cast on a silicon surface of 1 cm^2 (**Fig 1a**). To allow the adhesion of the protein the surface, the solution was left for 5 minutes in a closed chamber under N_2 flux (**Fig. 1b**). The process parameters used in the spinning phase (**Fig. 1c**) were optimized to give smooth thin films starting from our solutions. The maximum speed was set at 2000 rpm and the acceleration at 150 rpm/s, for a total spin coating time (both spinning **Fig 1c,** and evaporation **Fig. 1d**) of 55 s. These parameters were kept constant regardless the solution concentration and the solute typology (fibroin, sericin, FPP, or SPP). The evaporation step (**Fig. 1d**) was conducted at the maximum velocity of 2000 rpm for 42 s after the spinning ramp, to allow the complete removal of the solvent.

To evaluate the effect of the FPP and SPP exposure to UV radiation, 3 films for each type were exposed for 2 s to UV at 365 nm and 2 mW/cm^2 (Lumen Dynamics OmniCure 1000). The nomenclature used in section 2.2 has been maintained also for the films, with the only addition for resist films of the subscription Ex for exposed, and Unex for unexposed.

2.5. Characterization

Refractive index and thickness were obtained for each film using a Horiba UVISEL 460 spectroscopic ellipsometer, fitting 6 spectra for each protein/solvent combination (2 spectra for each of 3 films) with transparent Sellmeier and Cauchy models (formulae in **Tab. 1**). Surface morphology was obtained using a Zygo New View 6300 Optical Profilometer (OP) and NT-MDT Solver Nano Atomic Force Microscope (AFM). Secondary structures were obtained using an Fourier Transform Infrared spectroscope (FTIR) Nicolet Avatar 330 with a Diffuse Reflectance (DRIFT) accessory, subtracting the silicon as background. The fitting was conducted using a Fourier Self-Deconvolution[34] to individuate the peak positions and then fitting the peaks using a gaussian function to minimize χ^2. The percentage of area for each peak respect to the total area of the primary amide peak (1580-1720 cm^{-1}) has been taken as a measure of the specific structure content [35][36][37].

3. Results and Discussion

Film	Sellmeier Parameters $n(\lambda) = A + B\frac{\lambda^2}{\lambda^2 - {\lambda_0}^2}$			Cauchy Parameters $n(\lambda) = A + \frac{10^4 B}{\lambda^2} + \frac{10^9 C}{\lambda^4}$		
	A	B	λ_0	A	B	C
FPP/FA Ex	1.5	0.8	151	1.533	0.7	-0.02
SD FPP/FA Ex	0.2	0.2	16	0.002	0.1	0.3
FPP/FA Unex	1.3	1.0	150	1.528	0.82	-0.08
SD FPP/FA Unex	0.2	0.2	12	0.002	0.09	0.1
rSF/FA	1.8	0.5	189	1.527	0.55	0.3
SD rSF/FA	0.1	0.1	17	0.001	0.05	0.2
rSF/H_2O	1.82	0.53	164	1.533	0.43	0.2
SD rSF/H_2O	0.05	0.05	3	0.001	0.09	0.1
SPP/FA Ex	1.5	0.8	164	1.524	0.6	0.4
SD SPP/FA Ex	0.3	0.3	27	0.001	0.1	0.3
SPP/FA Unex	1.5	0.8	162	1.525	0.65	0.2
SD SPP/FA Unex	0.2	0.2	21	0.001	0.08	0.1
SN/FA	1.56	0.80	158	1.536	0.69	0.11
SD SN/FA	0.07	0.08	9	0.001	0.03	0.05

Tab. 1: Fitting parameters and their standard deviation (SD) for the two models used to calculate the refractive index n of silk films. Average fitting parameters and SD values were calculated from the results of different measurements on films of the same type.

The use of an optimized spin coating deposition on silicon substrate of a low concentration protein solution gives surfaces with an extremely low roughness even on a square millimeter scale. Films with these kinds of surfaces have been used to conduct ellipsometric measurements from 400 nm to 1500 nm. To fit the ellipsometric data, two models typically employed for transparent materials have been used, Sellmeier and Cauchy. Both models assume that the extinction coefficient k is zero at every wavelength, which in our case is very reasonable due to the negligible absorbance of our thin films out of the UV region [30]. The values of refractive index obtained with the two models are practically identical.

It is worth to note that RI of silk films prepared from the same batch and in the same conditions may be slightly different. This effect could be attributed both to the intrinsic variability of the secondary structure of the starting material (even inside the same batch from cocoon to cocoon) and to the environmental and preparation process variables. In order to take into account the reproducibility effects, we took 2 measurements on each of the 3 films prepared from the same protein in the same conditions, then the mean value and the standard deviation (SD) of both fitting parameters and RI were calculated from the values obtained with the different measurements. In this case, the standard deviation has to be considered as a measure that takes into account the reproducibility of our process, and not the precision of the single measurement.

3.1. Films morphology

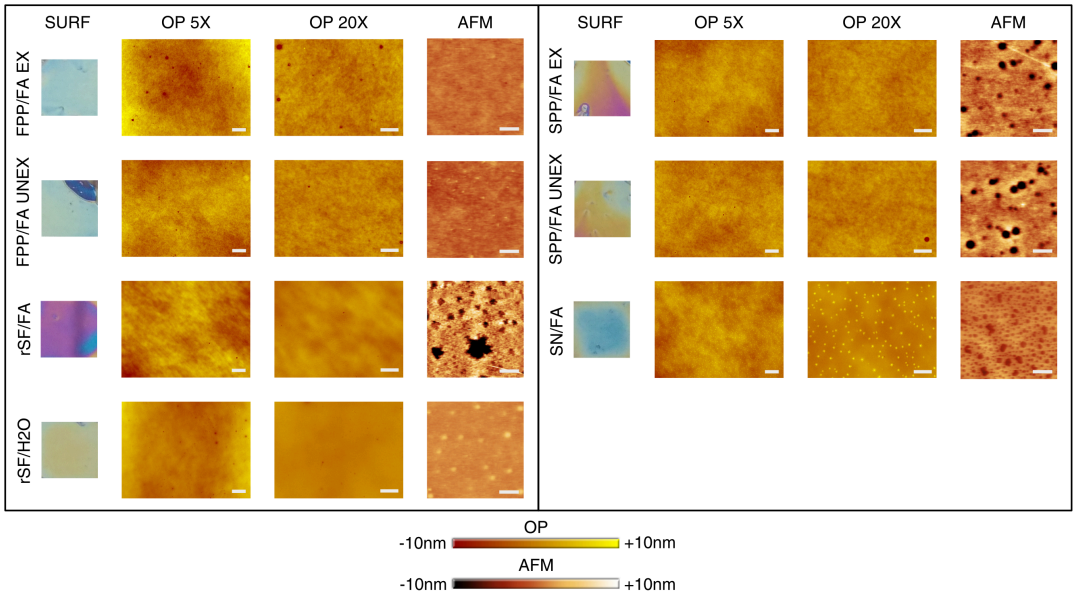

Fig. 2: Surface images (SURF) and Micrographies of silk protein films deposed by spin coating on silicon surfaces: Optical Profilometry at 5X (scale bar 150µm) and 20X (scale bar 50µm) magnification, and Atomic Force Microscopy (scale bar 2µm). Nanometric holes can be noticed at different scales in each sample. A fractal-like structure can be seen for SN/FA film in the OP taken at 20X. Despite the morphological features, all the surfaces result extremely smooth and allow a precise RI measurement via ellipsometry.

		OP 5X		OP 20X		AFM	
Film	Protein Conc. %	R_a [nm]	R_{rms} [nm]	R_a [nm]	R_{rms} [nm]	R_a [nm]	R_{rms} [nm]
FPP/FA Ex.	1.5	2.0	3.0	1.3	2.9	0.4	0.5
FPP/FA UnEx.	1.5	1.8	2.3	0.9	1.6	0.6	0.7
rSF/FA	2	1.9	2.6	0.8	1.1	2.3	3.3
rSF/H_2O	2	1.8	2.3	0.5	0.6	1.0	1.5
SPP/FA Ex.	1.5	1.4	1.9	1.2	0.9	1.7	2.8
SPP/FA UnEx.	1.5	1.2	1.7	1.0	2.9	1.9	3.1
SN/FA	2	1.4	1.8	0.9	1.3	0.9	1.9

Tab. 2: Surface roughness values (arithmetic R_a, and root mean square R_{rms}) calculated from the measured micrographies. Even on a large scale (OP 5x, surface of 1410 µm x 1010 µm) we obtained an R_{rms} lower than 10 nm, on a smaller scale (OP 20x, surface of 700 µm x 500 µm) lower than 3nm, and on the AFM scale lower than 3.5 nm. These values of roughness allow the use of the ellipsometry measurements for the determination of the RI.

In order to correctly model the RI from ellipsometric measurements, the surface roughness is a critical issue, in particular for non-glassy surfaces even a small roughness (above 5 nm) could

induce considerable errors [38]. Higher surface roughness (5 nm - 50 nm) produces light scattering which affects the ellipsometric results, making them difficult to fit with an affordable model.

Films micrography are shown in **Fig. 2** and in **Tab. 2** the average roughness (R_a) and the root mean square roughness (R_{rms}) are reported. We used optical profilometry (OP) to characterize the surface at a large scale (millimeter) and the AFM to repeat the characterization at a lower scale (micrometer). Using the optimized spin coating methodology, we were able to obtain films of silk protein with extremely smooth surfaces even over a large area. In particular, the average roughness and root mean square roughness were respectively lower than 3 nm and 10 nm on a surface area equal to 1410 μm x 1010 μm (OP 5x), 1.3 nm and 3 nm on a surface area equal to 700 μm x 500 μm (OP 20x), 2.3 nm and 3.5 nm on a surface area equal to 10 μm x 10 μm (AFM). It's worth of notice that the lower roughness value in the sub-nanometer range. The high R_{rms} value for some samples could be related to holes or bumps which are visible in the micrography. In fact, R_{rms} strongly depends on the presence of peak values that are squared in the roughness calculus [39].

Nanometric holes observed both in AFM and OP has been observed in the literature [4][32] for rSF films. We detected the presence of similar holes, at different scales, for all our samples, including silk resist and sericin films. Furthermore, a typical fractal self-assembly [40], usually observed in sericin films cast from water, can be seen in our samples for the sericin film from FA (SN/FA OP 20x).

3.2. Secondary Structure

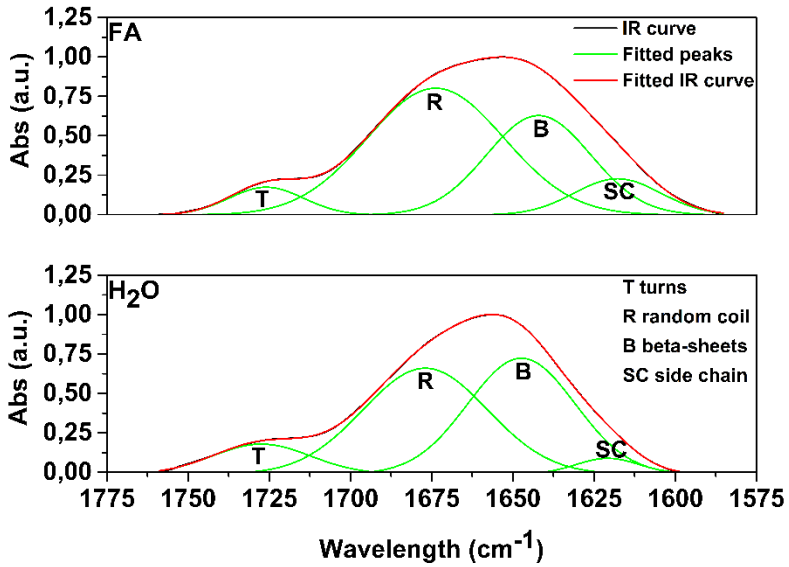

Fig. 3: Peaks fitting made on the infrared absorbance spectrum Amide I peak for secondary structure analysis. The area of the fitted peaks is correlated with the percentage of the assigned secondary structure. In our case, the relative amounts of ß-sheets and random coil structures has been used to evaluate the change in the RI due to the solvent effect. In water thin films an increase of beta-sheets and a decrease in random coils is detectable.

	FA		Water	
Structure	Wavelength (cm^{-1})	Area (%)	Wavelength (cm^{-1})	Area (%)
Turns	1618	9.5	1620	3.4
Beta-sheets	1642	31.5	1647	42.0
Random coils	1674	52.7	1676	44.7
Side chains	1726	6.3	1727	9.8

Tab. 3: Assigned peaks and relative area. ß-sheets and random coils variations are reasonably the cause of the increasing RI in water thin films when compared with FA based thin films. Crystalline beta-sheets structure content is higher films from water solutions, justifying the increase of RI with respect to FA films.

In **Fig. 3** is shown the deconvolution of the Amine I structure with peaks evidencing the beta-sheet structure of the films [34][35][36][37]. It should be noticed that nor the FTIR in Total Attenuated Reflectance neither the use of a Grazing Angle accessory gave a spectra with a signal level suitable for further analysis. Instead the signal of spectra produced by DRIFT FTIR was strong enough for a quantitative evaluation, then the method is here reported for the first time for the application on thin Silk protein films. In our case, the relative amounts of crystalline (ß-sheets) and amorph (random coil) is important to evaluate the variation of RI due to structural variation. The assigned peaks and spectra are shown both in **Fig. 3** and in **Tab. 3**. From this analysis, water based thin films have a

higher content of β-sheets structure (42%) and a lower content of random coil structure (45%) in comparison with FA based thin films where ß-sheets and random content are, respectively, 32% and 53%. This high content of ß-sheet structure in water solution of rSF has been reported in the literature for thin and ultrathin films produced by Spin Assisted Layer by Layer method (SA-LBL) [41]. The higher crystallinity in our films is probably due to the effect of the TPM surface treatment of the substrate, giving rise to a polar surface-protein interaction. The interaction can be partially suppressed when the solvent is FA, which coordinates the side groups of fibroin chain, thus preventing the interaction with the surface [31][42].

3.3. Refractive Index

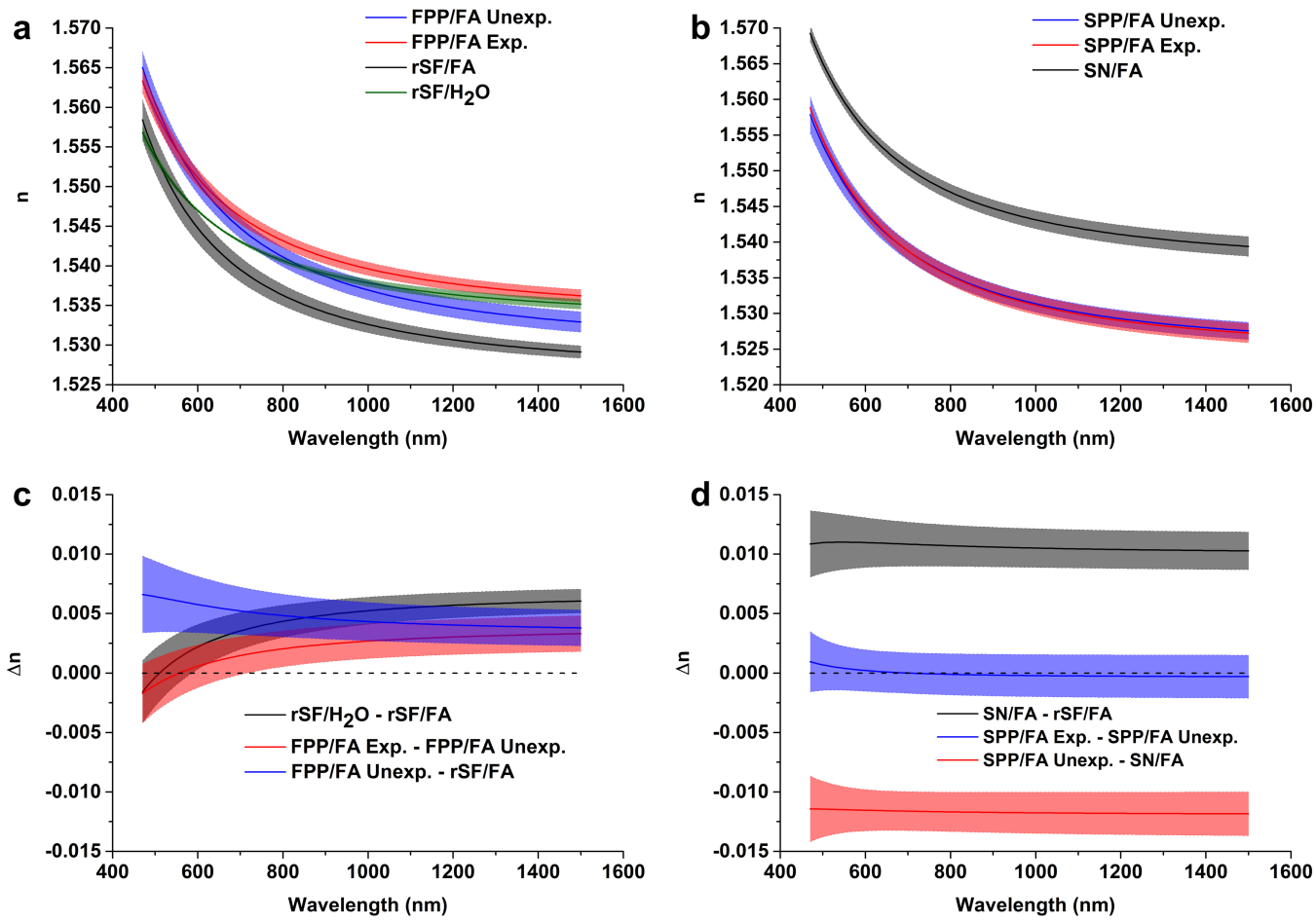

*Fig. 4: **a** and **b**, dispersion curves with error bars of RI for rSF/FA (a, black line), FPP/FA Unex (a, blue line), FPP/FA Ex (a, red line), SN/FA (b, black line), SPP/FA Unex (b, blue line) and SPP/FA Ex (b, red line). As can be noticed, the methacrylation process increases the RI for silk fibroin and decreases the RI for silk sericin. The UV exposure further increases the RI for FPP/FA films and*

*leaves unchanged the RI for SPP/FA films. **c** and **d**, RI difference and error bars as a function of the wavelength between different film typologies. A positive difference indicates that the first material can be used as lightguide when surrounded by the second material. On the contrary, a negative difference indicates the possibility to use the second material as lightguide when surrounded by the first one. A difference should be considered significant if the error bars does not intersect the 0 line (dashed black line).*

The refractive index is the most important parameter in the design of devices and sensors based on optical waveguides. The accurate knowledge of this parameter allows the correct design of optical components through ray-tracing when the wavelength is small if compared with the features dimensions, or through the resolution of Maxwell equations when the wavelength is comparable with the characteristic dimensions.

In **Fig. 4a,b** are reported the RI dispersion curves for the different films calculated with the interpolation of the ellipsometric data and the error bars are indicated by the bands surrounding the curves. The two models used for the interpolation, namely Sellmeier and Cauchy, gave the same results for the RI up to the forth decimal digit and for this reason only one value of RI is reported. In **Tab. 4** are reported RI values at the wavelengths typically reported in literature, that is 500 nm and 630 nm, in order to have a quick comparison between the different values. For instance, RI at 500 nm and 630 nm obtained for both fibroin thin films produced from water and from FA are in good agreement with data previously published[11][12][30][32][43]. In fact, at 630 nm the refractive index of rSF from water is 1.5456 and from FA is 1.5429, while for 500 nm the RI are 1.5537 and 1.5541, respectively. A striking difference on RI between thin films produced with the two solvents is observed only at higher wavelengths. The higher RI of rSF thin films obtained from aqueous solution, if compared with rSF/FA thin films, can be due to a slightly higher crystallinity. In fact, due to the higher density, crystalline protein structure gives reasonably a higher RI if compared to random conformation[30]. The increased crystallinity is reported for rSF/H_2O thin and ultrathin films deposed by spin-assisted Layer by Layer even without methanol treatment[41]. In our case, we can assume that the interaction with the TPM functionalized silicon surface with the protein groups induces an

increase of the crystalline fraction content. This effect is probably inhibited when the solvent is FA because it coordinates the rSF molecules better than water[31][42], thus limiting the protein-surface interaction.

In **Fig. 4 c,d** are reported the RI difference Δn curves between different materials, where the relative SD deviation are calculated with the error propagation formula. It should be noticed that we can consider the difference significant for a specific wavelength if the error bar does not overlap the 0 line. The RI variation (0.0064 at 500nm, 0.0022 at 630 nm) of FPP (FPP Unex, **Fig. 4a**, blue line) with respects to rSF is significant and can be related to the presence of methacrylate groups. A further small increment of RI (FPP Ex, **Fig. 4a**, red line) can be detected on FPP after the film exposure to UV light (-0.0010 at 500 nm, 0.0009 at 630 nm). This effect, detectable only for wavelength higher than 560 nm, where the two curves intersect, and significant after 700nm, can be attributed to a small increase in density due to the crosslinking process.

The measured RI for SN thin films (1.5651 at 500 nm, 1.5538 at 630 nm) made from FA is higher than the corresponding RI for rSF. The variation of RI (0.0110 at 500nm, 0.0109 at 630nm) is significant, suggesting the possible use of silk sericin in combination with fibroin in a core-cladding configuration. The methacrylation of silk sericin produces a significant decrement of RI (-0.0114 at 500 nm, -0.0116 at 630 nm), while no variation of RI has been detected after the UV exposure, as can be noticed from the fact that the 0 line stay within the RI curve error bar.

It has to be underlined that RI difference greater than or equal to 0.01 are suitable for the production of planar or fiber light guides [11][12]. For instance, it could be the case of sericin in combination with fibroin (rSF/FA – SN/FA Fig. 4d, solid line) or SPP (SPP Unex – SN/FA Fig. 4d, dotted line).

On the other hand, the RI difference between crosslinked and uncrosslinked FPP films (FPP Ex – FPP Unex **Fig. 4c**, dashed line), whose value is lower than 0.01 could be exploited to realize periodic structures interacting with UV light, such as photonic crystals [16][44][25] or Fiber Bragg Grating [45][46][47][48][49]. So, the results presented in this work evidence how

photocrosslinkable fibroin and sericine can be used for the fabrication of bio-compatible optical devices which can be used for sensing or inspecting bio-systems.

	Reference wavelengths						
Film	500 nm	630 nm	800 nm	1000 nm	1200 nm	1400 nm	1500 nm
FPP Ex	1.5595	1.5494	1.5432	1.5398	1.5377	1.5366	1.5362
SD FPP Ex	0.0013	0.0010	0.0009	0.0008	0.0008	0.0008	0.0008
FPP Unex	1.5605	1.5485	1.5411	1.5371	1.5347	1.5334	1.5329
SD FPP Unex	0.0018	0.0014	0.0012	0.0012	0.0012	0.0013	0.0013
rSF/FA	1.5541	1.5429	1.5363	1.5326	1.5307	1.5295	1.5291
SD rSF/FA	0.0024	0.0018	0.0013	0.0010	0.0009	0.0008	0.0008
rSF/H_2O	1.5537	1.5456	1.5406	1.5378	1.5364	1.5355	1.5352
SD rSF/H_2O	0.0005	0.0001	0.0003	0.0005	0.0005	0.0006	0.0006
SPP Ex	1.5543	1.5424	1.5352	1.5311	1.5290	1.5277	1.5272
SD SPP Ex	0.0004	0.0010	0.0012	0.0013	0.0013	0.0013	0.0013
SPP Unex	1.5536	1.5423	1.5353	1.5314	1.5293	1.5280	1.5275
SD SPP Unex	0.0021	0.0014	0.0012	0.0012	0.0012	0.0012	0.0012
SN/FA	1.5651	1.5538	1.5470	1.5431	1.5411	1.5398	1.5394
SD SN/FA	0.0010	0.0009	0.0011	0.0012	0.0013	0.0014	0.0014

Tab. 4: RI and SD of the measured typologies of thin films at different wavelengths. The two commonly used wavelengths (500 nm and 630 nm) for the characterization of silk fibroin are in good agreement with those reported in the literature

4. Conclusions

In this work, using a modified spin coating process, we were able to obtain exceptionally smooth silk films, with a very low roughness even at a large scale, suitable for RI characterization by ellipsometry. Sellmeier and Cauchy parameters were determined for thin films of silk protein resist (FPP and SPP), SN and, rSF, and the RI was then extracted in the 400 – 1500 nm range.

RI of thin films of rSF depends on the used solvent, it results to be a little bit higher starting from an aqueous solution than FA, ranging from 1.5456 at 630 nm to 1.5456 at 500 nm for water, and from 1.543 to 1.5429 for FA. This effect has been explained considering the secondary structure and the interaction of the protein with the TPM silicon surface. In particular, rSF thin films made starting

for water compared with FA made films shows a higher content of ß-sheets (42% vs 31.5%) structure and a lower content of random coil (44.7% vs 52.7%).

As a result of the chemical modification, RI of FPP (1.5605 at 500nm, 1.5485 at 630 nm) results higher than the RI of rSF. As effect of the crosslinking process and the consequent densification after UV exposure, the FPP films show a further little increment of RI that can be detected at wavelengths higher than 560 nm (1.5595 at 500 nm, 1.5494 at 630 nm).

SN RI (1.5651 at 500 nm, 1.5538 at 630 nm) has for the first time been characterized, and it slightly higher than the RI of rSF, suggesting the possibility of using SN and rSF in combination to produce a lightguide. SPP RI, (1.5536 at 500 nm, 1.5538 at 630 nm) as effect of the chemical modification of the SN protein, is lower than the SN RI. No further variation has been detected after the UV exposure of SPP films.

The evidence of the finite difference between the RI values of the different films allow to hypothesize possible application for these materials: in particular SN in conjunction with rSF could be feasible for realizing optical waveguides, while the RI modulation of FPP under UV irradiation could be exploited to realize periodical RI variation based devices, like fiber Bragg Gratings or photonic crystals.

Bibliography

[1] N. Kasoju, U. Bora, Silk fibroin in tissue engineering, Adv. Healthc. Mater. 1 (2012) 393–412. doi:10.1002/adhm.201200097.

[2] P. Bhattacharjee, B. Kundu, D. Naskar, H.-W. Kim, T.K. Maiti, D. Bhattacharya, S.C. Kundu, Silk scaffolds in bone tissue engineering: An overview, Acta Biomater. (2017). doi:10.1016/j.actbio.2017.09.027.

[3] M.A. Brenckle, B. Partlow, H. Tao, M.B. Applegate, A. Reeves, M. Paquette, B. Marelli, D.L. Kaplan, F.G. Omenetto, Methods and Applications of Multilayer Silk Fibroin Laminates Based on Spatially Controlled Welding in Protein Films, Adv. Funct. Mater. 26 (2016) 44–50. doi:10.1002/adfm.201502819.

[4] B. Kundu, N.E. Kurland, V.K. Yadavalli, S.C. Kundu, Isolation and processing of silk proteins for biomedical applications, Int. J. Biol. Macromol. 70 (2014) 70–77. doi:10.1016/j.ijbiomac.2014.06.022.

[5] X. Wang, D.L. Kaplan, Functionalization of Silk Fibroin with NeutrAvidin and Biotin, Macromol. Biosci. 11 (2011) 100–110. doi:10.1002/mabi.201000173.

[6] C. Vepari, D.L. Kaplan, Silk as a biomaterial, Prog. Polym. Sci. 32 (2007) 991–1007. doi:10.1016/j.progpolymsci.2007.05.013.

[7] B. Kundu, N.E. Kurland, S. Bano, C. Patra, F.B. Engel, V.K. Yadavalli, S.C. Kundu, Silk proteins for biomedical applications: Bioengineering perspectives, Prog. Polym. Sci. 39 (2014) 251–267. doi:10.1016/j.progpolymsci.2013.09.002.

[8] L.D. Koh, Y. Cheng, C.P. Teng, Y.W. Khin, X.J. Loh, S.Y. Tee, M. Low, E. Ye, H.D. Yu, Y.W. Zhang, M.Y. Han, Structures, mechanical properties and applications of silk fibroin materials, Prog. Polym. Sci. 46 (2015) 86–110. doi:10.1016/j.progpolymsci.2015.02.001.

[9] G.H. Altman, F. Diaz, C. Jakuba, T. Calabro, R.L. Horan, J. Chen, H. Lu, J. Richmond, D.L. Kaplan, Silk-based biomaterials, Biomaterials. 24 (2003) 401–416. doi:10.1016/S0142-9612(02)00353-8.

[10] L.-D. Koh, Y. Cheng, C.-P. Teng, Y.-W. Khin, X.-J. Loh, S.-Y. Tee, M. Low, E. Ye, H.-D. Yu, Y.-W. Zhang, M.-Y. Han, Structures, mechanical properties and applications of silk fibroin materials, Prog. Polym. Sci. 46 (2015) 86–110. doi:10.1016/j.progpolymsci.2015.02.001.

[11] S.T. Parker, P. Domachuk, J. Amsden, J. Bressner, J. a. Lewis, D.L. Kaplan, F.C. Omenetto, Biocompatible silk printed optical waveguides, Adv. Mater. 21 (2009) 2411–2415. doi:10.1002/adma.200801580.

[12] M.B. Applegate, G. Perotto, D.L. Kaplan, F.G. Omenetto, Biocompatible silk step-index optical waveguides, Biomed. Opt. Express. 6 (2015) 4221. doi:10.1364/BOE.6.004221.

[13] K. Hey Tow, D.M. Chow, F. Vollrath, I. Dicaire, T. Gheysens, L. Thevenaz, Exploring the use of native spider silk as an optical fibre for chemical sensing, J. Light. Technol. 8724 (2017) 1–8. doi:10.1109/JLT.2017.2756095.

[14] J.J. Amsden, A. Gopinath, L. Dal Negro, D.L. Kaplan, F.G. Omenetto, Silk Fibroin Biosensor Based on Imprinted Periodic Nanostructures, 2009 Conf. Lasers Electro-Optics Quantum Electron. Laser Sci. Conf. (Cleo/Qels 2009), Vols 1-5. 7 (2009) 201–202\n3405.

[15] Z. Zhou, Z. Shi, X. Cai, S. Zhang, S.G. Corder, X. Li, Y. Zhang, G. Zhang, L. Chen, M. Liu, D.L. Kaplan, F.G. Omenetto, Y. Mao, Z. Tao, T.H. Tao, The Use of Functionalized Silk Fibroin Films as a Platform for Optical Diffraction-Based Sensing Applications, Adv. Mater. 29 (2017) 1–7. doi:10.1002/adma.201605471.

[16] Q. Li, N. Qi, Y. Peng, Y. Zhang, L. Shi, X. Zhang, Y. Lai, K. Wei, I.S. Kim, K.-Q. Zhang, Sub-micron silk fibroin film with high humidity sensibility through color changing, RSC Adv. 7 (2017) 17889–17897. doi:10.1039/C6RA28460D.

[17] S.C. Kundu, B.C. Dash, R. Dash, D.L. Kaplan, Natural protective glue protein, sericin bioengineered by silkworms: Potential for biomedical and biotechnological applications, Prog. Polym. Sci. 33 (2008) 998–1012. doi:10.1016/j.progpolymsci.2008.08.002.

[18] M.N. Padamwar, A.P. Pawar, Silk sericin and its application : A review, J. Sci. Ind. Res. (India). 63 (2004) 323–329.

[19] Z. Wang, Y. Zhang, J. Zhang, L. Huang, J. Liu, Y. Li, G. Zhang, S.C. Kundu, L. Wang, Exploring natural silk protein sericin for regenerative medicine: an injectable, photoluminescent, cell-adhesive 3D hydrogel, Sci. Rep. 4 (2015) 7064.

doi:10.1038/srep07064.

[20] L. Lamboni, M. Gauthier, G. Yang, Q. Wang, Silk sericin: A versatile material for tissue engineering and drug delivery, Biotechnol. Adv. 33 (2015) 1855–1867. doi:10.1016/j.biotechadv.2015.10.014.

[21] N.E. Kurland, T. Dey, S.C. Kundu, V.K. Yadavalli, Precise Patterning of Silk Microstructures Using Photolithography, Adv. Mater. 25 (2013) 6207–6212. doi:10.1002/adma.201302823.

[22] N.E. Kurland, T. Dey, C. Wang, S.C. Kundu, V.K. Yadavalli, Silk protein lithography as a route to fabricate sericin microarchitectures, Adv. Mater. 26 (2014) 4431–4437. doi:10.1002/adma.201400777.

[23] R.K. Pal, N.E. Kurland, C. Wang, S.C. Kundu, V.K. Yadavalli, Biopatterning of silk proteins for soft micro-optics, ACS Appl. Mater. Interfaces. 7 (2015) 8809–8816. doi:10.1021/acsami.5b01380.

[24] W. Liu, Z. Zhou, S. Zhang, Z. Shi, J. Tabarini, W. Lee, Y. Zhang, S.N. Gilbert Corder, X. Li, F. Dong, L. Cheng, M. Liu, D.L. Kaplan, F.G. Omenetto, G. Zhang, Y. Mao, T.H. Tao, Precise Protein Photolithography (P3): High Performance Biopatterning Using Silk Fibroin Light Chain as the Resist, Adv. Sci. 1700191 (2017). doi:10.1002/advs.201700191.

[25] E. Colusso, G. Perotto, Y. Wang, M. Sturaro, F. Omenetto, A. Martucci, Bioinspired stimuli-responsive multilayer film made of silk–titanate nanocomposites, J. Mater. Chem. C. 5 (2017) 3924–3931. doi:10.1039/C7TC00149E.

[26] S. Kujala, A. Mannila, L. Karvonen, K. Kieu, Z. Sun, Natural Silk as a Photonics Component: a Study on Its Light Guiding and Nonlinear Optical Properties., Sci. Rep. 6 (2016) 22358. doi:10.1038/srep22358.

[27] S. Asha, Y. Sangappa, S. Ganesh, Tuning the Refractive Index and Optical Band Gap of Silk Fibroin Films by Electron Irradiation, J. Spectrosc. 2015 (2015) 879296/1-7. doi:10.1155/2015/879296.

[28] R. Madhukumar, S. Asha, B. Lakshmeesha Rao, B.K. Sarojini, K. Byrappa, Y. Wang, Y. Sangappa, Optical properties of γ-irradiated *Bombyx mori* silk fibroin films, Radiat. Eff. Defects Solids. 170 (2015) 906–915. doi:10.1080/10420150.2015.1136309.

[29] G. Perotto, M. Cittadini, H. Tao, S. Kim, M. Yang, D.L. Kaplan, A. Martucci, F.G. Omenetto, Fabrication of Tunable, High-Refractive-Index Titanate-Silk Nanocomposites on the Micro- and Nanoscale, Adv. Mater. 27 (2015) 6728–6732. doi:10.1002/adma.201501704.

[30] G. Perotto, Y. Zhang, D. Naskar, N. Patel, D.L. Kaplan, The optical properties of regenerated silk fibroin films obtained from different sources The optical properties of regenerated silk fibroin films obtained from different sources, 103702 (2017). doi:10.1063/1.4998950.

[31] I.C. Um, H.Y. Kweon, K.G. Lee, Y.H. Park, The role of formic acid in solution stability and crystallization of silk protein polymer, Int. J. Biol. Macromol. 33 (2003) 203–213. doi:10.1016/j.ijbiomac.2003.08.004.

[32] A. Bucciarelli, R.K. Pal, D. Maniglio, A. Quaranta, V. Mulloni, A. Motta, V.K. Yadavalli, Fabrication of Nanoscale Patternable Films of Silk Fibroin Using Benign Solvents, 201700110 (2017) 1–9. doi:10.1002/mame.201700110.

[33] D.N. Rockwood, R.C. Preda, T. Yücel, X. Wang, M.L. Lovett, D.L. Kaplan, Materials fabrication from Bombyx mori silk fibroin, Nat. Protoc. 6 (2011) 1612–1631.

doi:10.1038/nprot.2011.379.

[34] P.B. Tooke, Fourier self-deconvolution in IR spectroscopy, Trends Anal. Chem. 7 (1988) 130–136. doi:10.1016/0165-9936(88)87010-9.

[35] X. Hu, D. Kaplan, P. Cebe, Determining Beta-Sheet Crystallinity in Fibrous Proteins by Thermal Analysis and Infrared Spectroscopy, Macromolecules. 39 (2006) 6161–6170. doi:10.1021/ma0610109.

[36] E. Callone, S. Dirè, X. Hu, A. Motta, Processing Influence on Molecular Assembling and Structural Conformations in Silk Fibroin: Elucidation by Solid-State NMR, ACS Biomater. Sci. Eng. 2 (2016) 758–767. doi:10.1021/acsbiomaterials.5b00507.

[37] J.T. Pelton, L.R. McLean, Spectroscopic Methods for Analysis of Protein Secondary Structure, Anal. Biochem. 277 (2000) 167–176. doi:10.1006/abio.1999.4320.

[38] C. a. Fenstermaker, F.L. McCrackin, Errors arising from surface roughness in ellipsometric measurement of the refractive index of a surface, Surf. Sci. 16 (1969) 85–96. doi:10.1016/0039-6028(69)90007-7.

[39] T.R. Thomas, Characterization of surface roughness, Precis. Eng. 3 (1981) 97–104. doi:10.1016/0141-6359(81)90043-X.

[40] T.S. Khire, J. Kundu, S.C. Kundu, V.K. Yadavalli, The fractal self-assembly of the silk protein sericin, Soft Matter. 6 (2010) 2066. doi:10.1039/b924530h.

[41] C. Jiang, X. Wang, R. Gunawidjaja, Y.H. Lin, M.K. Gupta, D.L. Kaplan, R.R. Naik, V. V. Tsukruk, Mechanical properties of robust ultrathin silk fibroin films, Adv. Funct. Mater. 17 (2007) 2229–2237. doi:10.1002/adfm.200601136.

[42] I.C. Um, H. Kweon, Y.H. Park, S. Hudson, Structural characteristics and properties of the regenerated silk fibroin prepared from formic acid, Int. J. Biol. Macromol. 29 (2001) 91–97. doi:10.1016/S0141-8130(01)00159-3.

[43] G. Perotto, M. Cittadini, H. Tao, S. Kim, M. Yang, D.L. Kaplan, A. Martucci, F.G. Omenetto, Fabrication of Tunable , High-Refractive-Index Titanate – Silk Nanocomposites on the Micro- and Nanoscale, (2015). doi:10.1002/adma.201501704.

[44] Y.Y. Diao, X.Y. Liu, G.W. Toh, L. Shi, J. Zi, Multiple structural coloring of silk-fibroin photonic crystals and humidity-responsive color sensing, Adv. Funct. Mater. 23 (2013) 5373–5380. doi:10.1002/adfm.201203672.

[45] V. Rajoria, J. Singh, M. Tiwari, A. Khare, Design and Simulation of Optical Fiber Bragg Grating Using Refractive Index and Temperature, 2 (2011) 61–63.

[46] K.O. Hill, G. Meltz, Fiber Bragg grating technology fundamentals and overview, J. Light. Technol. 15 (1997) 1263–1276. doi:10.1109/50.618320.

[47] A.P. Zhang, S. Gao, G. Yan, Y. Bai, Advances in optical fiber bragg grating sensor technologies?, Photonic Sensors. 2 (2012) 1–13. doi:10.1007/s13320-011-0048-x.

[48] F. P., M. H., Photonic Structures in Biology: A Possible Blueprint for Nanotechnology, Nanomater. Nanotechnol. 4 (2014) 1–12. doi:10.5772/58289.

[49] P. Henzi, D.G. Rabus, Y. Ichihashi, M. Bruendel, J. Mohr, Photonic integrated polymer components and circuits by UV-induced refractive index modification, 6185 (2006) 618502. doi:10.1117/12.673843.